

## **Supporting Information**

### **The Efficient Degradation and Mechanism of Sulfamethoxazole using ZnO/ZnIn<sub>2</sub>S<sub>4</sub> Heterojunction under Visible Light**

Xinhong Gan<sup>1</sup>, Yang Song<sup>2</sup>, Guoqiang Liu<sup>1</sup>, Huijuan Zhang, Jianhua Yang<sup>2\*</sup>

<sup>1</sup> State Environmental Protection Key Laboratory of Soil Environmental Management and Pollution Control, Nanjing Institute of Environmental Science, Ministry of Ecology and Environment (MEE) of China, Nanjing 210042 (China).

<sup>2</sup> Anhui University of Technology, School of Energy and Environment, Maanshan 243002, Anhui, Peoples R China.

\*Corresponding author: Jianhua Yang (E-mail:yangjh@ahut.edu.cn

Phone: 86-0555-2312885; Fax: 86-0555-2312885 )

**11 Texts**

**5 Tables**

**13 Figures**

**29 Pages**

## **Contents:**

**Text S1** Methods for the preparation of ZnO and ZnO/ZIS.

**Text S2** Characterization methods of ZnO/ZIS.

**Text S3** Experimental analysis method.

**Text S4** The analysis of SEM-EDS、TEM、BET.

**Text S5** The analysis of XRD and XPS.

**Text S6** The analysis of Zeta potential.

**Text S7** The analysis of UV-vis、PL and Photocurrent.

**Text S8** The adsorption of SMX on ZnO/ZIS.

**Text S9** Influencing Factors of SMX by ZnO/ZIS.

**Text S10** Anion Effect on the degradation of SMX by ZnO/ZIS.

**Text S11** Mineralization Rate, Stability and Cyclic Experiment.

**Table S1** Gradient elution conditions

**Table S2** BET data for ZnO, ZIS, ZnO/ZIS

**Table S3** Structure of degradation products

**Table S4** The absolute energy of P9a gas molecules, the absolute energy and adsorption energy of P9a on ZnO(001)/ZnIn<sub>2</sub>S<sub>4</sub>(102) heterojunction surface

**Table S5** Leaching rate of metal ions after degradation of SMX by ZnO/ZIS

**Figure S1** Schematic diagram of preparation process of ZnO/ZIS.

**Figure S2** SEM image (a); TEM image (b); EDS layered image (c)(d)(e)(f) of ZnO/ZIS.

**Figure S3** Nitrogen adsorption-desorption isotherms (a) and pore size distribution map (b) of ZnO, ZIS, ZnO/ZIS.

**Figure S4** XRD patterns of ZnO, ZIS, ZnO/ZIS.

**Figure S5** XPS spectra of ZnO/ZIS heterostructure, (a) survey of the sample, (b) Zn 2p, (c) In 3d, (d) S 2p and (e) O 1s.

**Figure S6** TGA (a) and Zeta potentials (b) of ZnO, ZIS and ZnO/ZIS.

**Figure S7** (a) The i-t diagrams of ZIS and ZnO/ZIS and (b) the photoluminescence spectra of ZnO, ZIS and ZnO/ZIS at an excitation wavelength of 376 nm.

**Figure S8** (a) Photodegradation kinetics and dark adsorption process of SMX under 500 w visible light, (b) The Kobs of SMX degradation by ZnO/ZIS.

Condition:  $[\text{SMX}]_0=2.5$  mg/L, 0.20 g/L dosage, pH=5.0, 500 w, 15-20°C.

**Figure S9** Effect of common anions and humic acids in water on the degradation of SMX(a)(b) by ZnO/ZIS. Conditions: (a)(b)  $[\text{SMX}]_0=2.5$  mg/L, 0.20 g/L dosage, pH=5.0, 500 w, room temperature.

**Figure S10** The mass spectrum data and possible structures of 9 main products after ZnO/ZIS-5 degradation of SMX.

**Figure S11** Mass spectrum of degradation product P10 of SMX.

**Figure S12** The mineralization rate of ZnO/ZIS photocatalytic degradation of SMX.

**Figure S13** The degradation efficiency of SMX using only ZnO and only ZnIn<sub>2</sub>S<sub>4</sub>.

**Figure S14** The influence of light source intensity on the degradation of SMX by ZnO/ZnIn<sub>2</sub>S<sub>4</sub>.

### **Text S1 Methods for the preparation of ZnO and ZnO/ZIS.**

Dissolve zinc acetate, urea and sodium citrate in deionized water at a certain molar ratio, magnetic stirring for 30 min, place them in a 100 mL high-pressure reactor, and hydrothermal reaction at 120°C for 6 h. After centrifugation, the precipitates were collected, washed three times with deionized water and absolute ethanol, and dried in an oven at 80°C. Then the dried white powder is sent to the muffle furnace and calcined at 300°C for 2 h to obtain pure ZnO powder.

Firstly, weigh zinc sulfate, indium chloride and thioacetamide to ensure that their molar ratio is 1:2:8, and add deionized water for ultrasonic dissolution. Then add 0.06 g of ZnO powder to the above solution, disperse it evenly by ultrasonic, place it in an autoclave and heat it at 160°C for 16 h. The yellow precipitate after hydrothermal reaction is collected, centrifuged and washed with deionized water and absolute ethanol for three times, and then dried in a vacuum drying oven to obtain the yellow powder of ZnO/ZIS. The schematic diagram of preparation process of ZnO/ZIS is exhibited in Figure S1.

### **Text S2 Characterization methods of ZnO/ZIS.**

The surface morphology of photocatalysts were observed on the scanning electron microscope (SEM) of JSM-7800F and the transmission electron microscope (TEM) of JEM-2100 (Japan Electronics). The specific surface area of the sample was tested on ASAP 2460 (American Mike). The parameters such as crystal plane spacing and crystallinity were analyzed by X-ray diffraction (XRD) of D8 ADVANCE (Brooke, Germany). X-ray photoelectron spectroscopy (XPS) is performed on a

K-Alpha (Thermo Scientific) spectrometer.

The zeta potential data of ZnO/ZIS catalyst were determined by Malvern Zeta sizer Nano ZS90 (UK). Taking BaSO<sub>4</sub> powder as the reference, the wavelength range was 400-800 nm, and the UV-vis diffuse reflection spectrum (UV-vis) was obtained on the UV-vis spectrophotometer of model UV3600 (Shimadzu, Japan). Photoluminescence(PL) spectra were measured with steady-state/transient fluorescence spectrometer of FLS1000 (Edinburgh) at an excitation wavelength of 376 nm. To determine the photocurrent performance of the samples, an electrochemical workstation with model CHI760E was used for testing. The counter electrode is platinum wire, the reference electrode is Ag/AgCl, and the catalyst powder is deposited on tin fluoride oxide (FTO) glass as the working electrode. Using a quartz electrolytic cell containing 50 mL 0.1 M Na<sub>2</sub>SO<sub>4</sub> as the reaction system, the test was carried out under the condition of 300 W xenon lamp (CEL-PF300-T8, Beijing Zhongjiao Jinyuan) as the visible light source.

Open circuit potential (OCP): Electrochemical analysis was conducted at the electrochemical workstation (Shanghai Chenhua 760E). The experiment was conducted using a three electrode structure, with the working electrode, platinum electrode as the counter electrode, and Ag/AgCl electrode as the reference electrode. In the preparation of the working electrode, 10 mg of catalyst was mixed with 1 mL of ethanol and 10  $\mu$ L Nafion solution and sonicate for 30 minutes. Then drip FTO conductive glass (spin coated area of 1 $\times$ 2 cm<sup>2</sup>), the method is to place the prepared FTO glass on a spin coating machine and first drop 10  $\mu$ L. Turn on the spin coating machine switch and add 10  $\mu$ L when rotating slowly. Cover and rotate quickly. After the spin coating is completed, place the FTO glass on a heating table and heat it at

150 °C for ten minutes. After it cools down, repeat this step three times. Finally, remove the adhesive tape from the glass and heat it at 350 °C for 30 minutes. The electrolyte is a Na<sub>2</sub>SO<sub>4</sub> aqueous solution (1 M). Monitor the open circuit potential time in the sodium sulfate electrolyte using SMX.

Measure the open circuit potential (OCP) of the FTO coated electrode without applying external voltage. As shown in the figure, the xenon lamp is used for 0-100 seconds and the xenon lamp is turned off for 100-300 seconds. With the addition of SMX solution, the OCP increases sharply, and the reason for this phenomenon is that SMX first interacts with the catalyst, and some electrons transferred from the catalyst to SMX increase the oxidation potential of the catalyst.

### **Text S3 Experimental analysis method.**

Photocatalytic Degradation of SMX. The photocatalytic degradation experiment was operated by Shanghai Zhengqiao ZQ-GHX-V photocatalytic reactor. At the beginning of each experiment, a certain quality of ZnO/ZIS photocatalyst and 50 mL of SMX solution were placed in a quartz tube, a magnetic stirrer was put into, and stirred continuously in the dark for 30 min. Next, a 500 w xenon lamp (380 nm-780 nm) was used to simulate the visible light source of the degradation process, and the touring device was turned on to ensure that the solution can receive light uniformly. At the designed time point, 2 mL of solution was taken out and filtrated through 0.45 μm filter head for subsequent determination and analysis of concentration.

The solution concentration was measured and analyzed by TU-1901 double beam UV-Vis spectrophotometer, the concentration of SMX was measured at 240 nm. TOC-L CPN total organic carbon analyzer was used to determine the total organic carbon value (TOC) of the solution before and after the degradation of SMX by ZnO/ZIS for 6.5h.

The degradation products of SMX were determined by liquid chromatography/mass spectrometry (LC-MS). The chromatographic model was a Dionex Ultimate 3000 UHPLC, and the mass spectrometer model was a Thermo Scientific Q Exactive. The chromatographic column was Accucore Vanquish C18+ (column length×inside diameter, 100 mm×2.1 mm), and the injection volume was 5.0  $\mu$ L. The mobile phase was 0.1% formic acid water-0.1% formic acid acetonitrile. The gradient elution conditions are shown in Table S1. The positive ion mode HESI ion source was used for mass spectrometry, and the m/z scanning range was 50-750. The gas lift rate was 40 mL/min, the auxiliary gas rate was 10 mL/min, the spray voltage was 3 kV, and the capillary temperature was 300°C.

The EPR test was carried out on a Bruker EMX PLUS spectrometer in Germany, and a 300-W xenon lamp was used to simulate a visible light source. Typical test parameters are: sweep width 100.0 G, sweep time 30.0 s, modulation amplitude 3.00 G, modulation frequency 100.0 kHz. When ZnO/ZIS degrades SMX, solutions are taken 30 min, 60 min, 120 min, 210 min and 270 min after the light reaction, and solutions are taken 15 min, 30 min, 60 min, 120 min and 270 min after the light reaction for qualitative and quantitative analysis.

## Computational method

We have employed the Vienna Ab Initio Package (VASP) to perform all the density functional theory (DFT) calculations within the generalized gradient approximation (GGA) using the PBE formulation. We have chosen the projected augmented wave (PAW) potentials to describe the ionic cores and take valence electrons into account using a plane wave basis set with a kinetic energy cutoff of 400 eV. Partial occupancies of the Kohn–Sham orbitals were allowed using the Gaussian smearing method and a width of 0.05 eV. The electronic energy was considered self-consistent when the energy change was smaller than  $10^{-5}$  eV. A geometry optimization was considered convergent when the force change was smaller than 0.02 eV/Å. Grimme’s DFT-D3 methodology was used to describe the dispersion interactions.

The equilibrium lattice constants of wurtzite-type Zn unit cell were optimized, when using a  $15 \times 15 \times 9$  Monkhorst-Pack k-point grid for Brillouin zone sampling, to be  $a=3.272$  Å,  $c=5.291$  Å. And the equilibrium lattice constants of hexagonal  $\text{ZnIn}_2\text{S}_4$  unit cell were optimized, when using a  $9 \times 9 \times 1$  Monkhorst-Pack k-point grid for Brillouin zone sampling, to be  $a=3.891$  Å,  $c=24.508$  Å. We then use both to construct a  $\text{ZnO}(001)/\text{ZnIn}_2\text{S}_4(102)$  heterojunction surface model. In the heterojunction, the  $\text{ZnO}(001)$  part has a  $p(8 \times 2\sqrt{3})$  periodicity and the  $\text{ZnIn}_2\text{S}_4(102)$  part has a  $p(8 \times 2\sqrt{3})$  periodicity, which insures the lattice mismatch as small as 3%. The  $\text{ZnO}(001)/\text{ZnIn}_2\text{S}_4(102)$  slab was separated by a vacuum layer in the Z direction in the depth of 15 Å in order to separate the surface slab from its periodic duplicates. This

model comprises of 76 Zn, 64 O, 24 In and 48 S atoms. During structural optimizations, the  $\Gamma$  point in the Brillouin zone was used for k-point sampling, and all atoms were allowed to relax.

The adsorption energy ( $E_{\text{ads}}$ ) of adsorbate A was defined as

$$E_{\text{ads}} = E_{A/\text{surf}} - E_{\text{surf}} - E_{A(\text{g})}$$

where  $E_{A/\text{surf}}$ ,  $E_{\text{surf}}$  and  $E_{A(\text{g})}$  are the energy of adsorbate A adsorbed on the surface, the energy of clean surface, and the energy of isolated A molecule in a cubic periodic box with a side length of 20 Å and a  $1 \times 1 \times 1$  Monkhorst-Pack k-point grid for Brillouin zone sampling, respectively.

#### **Text S4 The analysis of SEM-EDS, TEM, BET.**

As depicted in Figure S2, SEM (a), TEM (b) and EDS layered images (c) (d) (e) (f) can confirm the morphology and structure of ZnO/ZIS. It could be clearly seen that ZnO/ZIS composite catalyst is composed of flower shaped microspheres with a diameter of about 1  $\mu\text{m}$ . By observing image of Figure S2 (c) (d) (e), it can be found that the distribution of O element overlaps with that of Zn element, indicating that ZnO is successfully loaded on ZIS. It is easy to see that the stripe spacing of 0.267 nm corresponds to the (002) lattice plane of ZnO in the XRD figure; The crystal plane spacing  $d$  of ZIS is 0.320 nm, homologous the (102) crystal face of ZIS in XRD (Figure S4). In terms of position, the (002) crystal plane of ZnO overlaps with the (102) crystal surface of ZIS, which again confirms the conclusion that ZnO has been successfully loaded on ZIS.

As we know, BET is one of the vital factors to improve the reaction activity of

photocatalyst. Figure S3 (a) presents the N<sub>2</sub> adsorption-desorption curves of ZnO, ZIS and ZnO/ZIS, it can be judged that ZnO is a type III adsorption isothermal curve; Both ZIS and ZnO/ZIS are type II adsorption isotherms. Figure S3 (b) shows the pore size distribution of the photocatalysts, the pore sizes of ZnO most are above 10 nm, while the pore sizes of ZIS and ZnO/ZIS are mostly focused on 5 nm around. The other analysis parameters of BET are exhibited in Table S2, it could be clearly seen that the surface areas of ZIS and ZnO/ZIS are significantly larger than that of pure ZnO. The results verified that ZnO/ZIS composite photocatalyst could provide more contact sites and effectively improve the photocatalytic reaction rate.

#### **Text S5 The analysis of XRD and XPS.**

In order to explore the crystal structure and crystallinity of ZnO/ZIS, the photocatalyst was characterized by XRD in Figure S4. Pure ZIS has five diffraction peaks at 21.6°, 27.7°, 47.2°, 52.4° and 55.6°, corresponding to (006), (102), (110), (116) and (022) crystal planes of hexagonal ZIS (JCPDS#89-3963) respectively. For unmixed ZnO, its X-ray diffraction peak positions are 31.7°, 34.4°, 36.2°, 47.5°, 56.5°, 62.8°, 67.9° and 69.0° separately, which could well correspond to (100), (002), (101), (102), (110) (103), (112) and (201) surfaces of ZnO (JCPDS#89-1397). After the combination of ZIS and ZnO, the location of diffraction peaks were basically the same as that of simple ZIS, yet shifted to the right by 0.5° at (022), which may resulted from the position offset of the diffraction peak by the composite with ZnO. As Figure S4 shown, compared with the peaks of ZnO, the peaks of ZnO/ZIS-5 was indeed not obvious on the 101 side. We speculate that it may be due to the small

proportion of ZnO (5% wt) in composite ZnO/ZIS-5, resulting in data being drowned out during the characterization process. The peaks of ZIS and ZnO/ZIS-5 are basically consistent, with slight changes in peak intensity. The crystal peak area and total area of ZnO/ZIS were calculated by Origin as 1172.18 and 1572.68 respectively, then the crystallinity was computed via formula (1). The calculated crystallinity is 74.53%, indicating that the crystallinity of ZnO/ZIS is good and there are few impurities in ZnO/ZIS.

$$\text{Crystallinity} = \frac{\text{Crystal peak area}}{\text{Total area (crystal+amorphous)}} \times 100 = \frac{1172.18}{1572.68} \times 100 = 74.53 \% \quad (1)$$

XPS was further applied to survey the chemical state of each component of ZnO/ZIS composite photocatalyst, and the results are displayed in Figure S5. It shows the general spectrum of ZnO/ZIS, it proved that the composite photocatalyst is mainly composed of Zn, O, In and S. The XPS peaks of Zn 2p at 1021.96 eV and 1045.18 eV (Figure S5) relate to Zn 2p<sub>3/2</sub> and Zn 2p<sub>1/2</sub>, respectively. The XPS spectra of In 3d exhibit two peaks at 445.03 eV and 452.58 eV, which attribute to In 3d<sub>5/2</sub> and In 3d<sub>3/2</sub> energy levels. The asymmetric S 2p peak is divided into two sub-peaks at 161.78 eV and 162.98 eV, corresponding to S 2p<sub>3/2</sub> and S 2p<sub>1/2</sub>, respectively. The asymmetric O 1s peak is separate into two peaks at 532.06 eV and 533.58 eV, which match to O<sup>2-</sup> in the lattice and oxygen in the adsorbed state, respectively. The above analysis confirm that the chemical valence states of ZnO/ZIS are Zn<sup>2+</sup>, O<sup>2-</sup>, In<sup>3+</sup> and S<sup>2-</sup>.

#### **Text S6 The analysis of Zeta potential.**

The stability of ZnO/ZIS was investigated through characterization of zeta potential. Figure S6 displays the zeta potential of ZnO/ZIS in aqueous solutions with

different pH. As shown in the figure, the zeta potential values of ZnO/ZIS are negative when pH between 2-10, and the absolute value of zeta potential when  $\text{pH} \geq 6$  is basically maintained at about 33. The larger the absolute value of zeta potential value, the more stable the system is, which illustrates that the stability of ZnO/ZIS in aqueous solution is better with the gradual increase of pH value. In addition, zeta potential could also reveal the adsorption mechanism between catalyst and pollutants. The pKa values of SMX are 1.7 and 5.7. Thus, when  $\text{pH} \leq 1.7$ , SMX is positively charged. When  $\text{pH} \geq 5.7$ , SMX is negatively charged. ZnO/ZIS photocatalyst is negatively charged in the range of  $\text{pH} = 2-10$ , indicating that the adsorption of SMX by ZnO/ZIS does not belong to the category of physical adsorption when pH is between 2 to 10.

#### **Text S7 The analysis of UV-vis, PL and Photocurrent.**

As depicted in Figure 1ab, the absorption properties for visible light and band gap of ZnO, ZIS and ZnO/ZIS by UV-vis diffuse reflection spectroscopy were studied. Compared with pure ZnO, the absorption performance for visible light of ZnO/ZIS was significantly improved in the wavelength range of 400-800 nm. Moreover, ZnO/ZIS has higher utilization of visible light in the wavelength range of 520-800 nm than simple ZIS. It was also obvious from the figure that the curve of ZnO/ZIS is basically between unmixed ZnO and ZIS, demonstrating the formation of heterojunction. Furthermore, according to the classical Tauc-Plot calculation method, the band gaps of ZIS and ZnO were calculated respectively. The calculation formula is as follows:

$$\alpha_{hv} = A(h\nu - E_g)^n \quad (2)$$

Where  $\alpha$ 、  $h$ 、  $\nu$ 、  $A$  and  $E_g$  stand for the absorption coefficient, planck constant, frequency, constant and band gap, separately. The index  $n$  is related to the type of semiconductor,  $n=1/2$  for direct band gap semiconductors and  $n=2$  for indirect band gap semiconductors. In addition,  $h\nu$  in equation (2) was got through equation (3):

$$h\nu = hc / \lambda \quad (3)$$

Where  $c$  is the speed of light,  $\lambda$  is the wavelength of light. According to the above formula, the band gap widths of ZnO, ZIS and ZnO/ZIS are 3.14 eV, 2.47 eV and 2.07 eV, severally. The results indicate that the band gap of the composite catalyst becomes narrower, which indirectly verifies that the visible light absorption capacity of ZnO/ZIS is enhanced. To better explain the cases of electron migration after ZnO and ZIS composite to form heterojunction, the valence band (VB) and conduction band (CB) of ZIS and ZnO were estimated following the empirical formula.

$$E_{VB} = X - E^0 + 0.5E_g \quad (4)$$

$$E_{CB} = E_{VB} - E_g \quad (5)$$

Where  $E_{VB}$  and  $E_{CB}$  mean the valence band potential and conduction band potential of the semiconductor, severally, and  $X$  is absolute electronegativity.  $E_0$  represents the free electron energy on the hydrogen scale, also known as the hydrogen scale (about 4.5 eV). Each  $X$  values of ZIS and ZnO are 4.87 eV and 5.95 eV. Therefore, the valence band potential and conduction band potential of ZIS are 1.64 eV and -0.87 eV respectively, the valence band potential and conduction band potential of ZnO are 3.02 eV and -0.12 eV, individually .

The photocurrent time (i-t) diagram (Figure S7a) and fluorescence spectrum

(Figure S7b) were measured to reveal the separation ability and recombination situation of photogenerated carriers of the materials, respectively. It was clearly seen that the photocurrent increases or decreases suddenly with the visible light source is turned on or off. At the same time, the photocurrent produced by ZnO/ZIS is greater than that of ZIS, which illustrates that the separation ability of photogenerated carriers of ZnO/ZIS is relatively good. In addition, the fluorescence intensity of each sample at the same excitation wavelength were tested. Theoretically, the higher fluorescence intensity, the higher recombination rate of photogenerated carriers. It can be seen from the figure that when the excitation wavelength is 376 nm, an emission peak produced by ZnO/ZIS at the wavelength of 652 nm, an emission peak generated on ZnO at the wavelength of 521 nm. Compared with ZnO and ZIS, the photogenerated carrier recombination rate of ZnO/ZIS is significantly reduced, which is consistent with the experimental results of photocurrent.

#### **Text S8 The adsorption of SMX on ZnO/ZIS.**

It is necessary to eliminate the effect of adsorption on the degradation of SMX. Consequently, the adsorption equilibrium experiment was designed before the degradation test, and the results are shown in Figure S8a. It can be seen from the figure that after the adsorption of SMX by ZnO/ZIS for 30 min, the removal efficiency of SMX is about 3.4%, and the adsorption process basically reaches to equilibrium. ZnO/ZIS has little adsorption on SMX. Therefore, the adsorption time before photodegradation process was set to 30 min, and all the photodegradation experiments were carried out on this time basis throughout this dissertation.

### **Text S9 Influencing Factors of SMX by ZnO/ZIS.**

In the influencing factors trial, SMX solution with initial concentration of 10 mg/L and pH=5.25 was applied as the research object to explore the effect of catalyst dosage on the degradation of SMX by ZnO/ZIS. As shown in Figure 2a, with the gradual increase of catalyst dosage, there was no obvious effect on the photocatalytic degradation efficiency of SMX, and the degradation effect of SMX reached an average of 60%. Merely, combined with the reaction rate and the degradation efficiency of SMX at 6.5 h, the degradation effect of SMX could reach 65% when the dosage of ZnO/ZIS was 0.20 g/L. Secondly, when the dosage was 0.30 g/L, the degradation efficiency of SMX was slightly lower than 0.2 g/L, while the dosage of 0.40 g/L had the worst degradation effect on SMX. Considering practical production and application, adhering to the concept of cost saving, the experimental conditions of this research content select the dosage of ZnO/ZIS as 0.2 g/L.

Based on the catalyst dosage of 0.2 g/L, the effects of five different concentrations of 2.5 mg/L, 5 mg/L, 10 mg/L, 20 mg/L and 40 mg/L on the photocatalytic degradation of SMX by ZnO/ZIS were studied as displayed in Figure 2b. When the initial concentration of SMX was greater than 2.5 mg/L, the degradation effect of SMX was poor, and the degradation efficiency also showed a downward trend with the increase of concentration. Furthermore, the best degradation effect of SMX can be achieved when the initial concentration of SMX was 2.5 mg/L, and the degradation efficiency was 72.5% after 6.5 hours of visible light irradiation. When the initial concentration of SMX increased to 40 ppm, the reaction rate slowed down and

the degradation effect of SMX was the worst, only 44.8% of SMX could be degraded. There are two possible reasons for the initial concentration has a great impact on the degradation efficiency of SMX, on the one hand, high initial concentration of SMX will increase the photon path length of the reaction system and affect the speed of visible light energy reaching the catalyst surface, thus hindering the process of photocatalytic reaction. On the other hand, intermediate products will be produced in the process of photodegradation, and the intermediate products will compete with SMX for active sites. As the reaction continues, the number of intermediates is also increasing, resulting in further intensification of competition. According to the above indexes, the optimal initial concentration of SMX was choosed by 2.5 mg/L.

The effect of pH value of SMX on photodegradation process is also apparently. Figure 2c presents the degradation effect of SMX by ZnO/ZIS with different pH value. when the pH value of SMX was 5.0, the degradation effect of SMX was as high as 74.0%. Taking pH = 5.0 as the dividing point, increasing or decreasing the pH of the SMX solution will both reduced the degradation efficiency of SMX, but the total degradation efficiency can be maintained at more than 60%. Since the adsorption of SMX on ZnO/ZIS was very weak, the influence of adsorption on photocatalytic degradation process was ignored here.

Xenon lamp power also plays a role in the degradation process of SMX. Due to the limitation of the function of the experimental equipment, 100 w, 300 w and 500 w xenon lamps were selected for degradation trials under the same other parameters, the specific effects are displayed in Figure 2d. When the xenon lamp power increased

from 100 w to 500 w, the degradation effect of SMX by ZnO/ZIS was significantly improved, while the degradation effect of SMX was the worst with the 100 w xenon lamp, and only 42.7% of SMX could be degraded. It can be seen that within a certain range, when xenon lamp is used as visible light source, xenon lamp power is still one of the main factors affecting the degradation of SMX, which is consistent with the previous research conclusions.

#### **Text S10 Anion Effect on the degradation of SMX by ZnO/ZIS.**

Figure S10 exhibits the photocatalytic degradation results of 2.5 mg/L SMX by ZnO/ZIS when 10 mg/L four inorganic anions ( $\text{HCO}_3^-$ ,  $\text{SO}_4^{2-}$ ,  $\text{NO}_3^-$ ,  $\text{PO}_4^{3-}$ ) and HA were added to SMX solution, severally. The order of photodegradation efficiency of SMX was  $\text{SO}_4^{2-} \approx \text{HA} \approx \text{NO}_3^- > \text{HCO}_3^- > \text{PO}_4^{3-}$ , it suggested that the presence of  $\text{NO}_3^-$ ,  $\text{SO}_4^{2-}$  and HA may had little or no effect on the photodegradation of SMX. As for  $\text{NO}_3^-$  played a weak role in promoting the degradation of SMX, it may be that the photolysis of low concentration  $\text{NO}_3^-$  will produced a small amount of hydroxyl radical ( $\cdot\text{OH}$ ), which can non-selectively oxidize some pollutants. In addition, according to some studies, HA can adsorb solar energy to produce free radicals, which may attack SMX molecules or their degradation by-products in water, HA promotes the photocatalytic system at this moment.

$\text{HCO}_3^-$  has obvious inhibitory effect on the photodegradation process of SMX, and the inhibitory effect will be more obvious with the increase of  $\text{HCO}_3^-$  concentration. There are two reasons for its inhibition, first, the hydrolysis of  $\text{HCO}_3^-$  produces a certain amount of  $\text{OH}^-$  and  $\text{HCO}_3^-$ , and the pH of aqueous solution

increases, resulting in the reduction of degradation efficiency of SMX. Second, the presence of  $\text{HCO}_3^-$  will consume  $\text{h}^+$  and  $\cdot\text{OH}$ , leading to the poor photocatalytic activity. There are three pKa values of  $\text{PO}_4^{3-}$ ,  $\text{pK}_{\text{a}1}=2.1$ ,  $\text{pK}_{\text{a}2}=7.2$  and  $\text{pK}_{\text{a}3}=12.3$ . Therefore, in the process of the degradation of SMX,  $\text{PO}_4^{3-}$  mainly exists in the form of  $\text{H}_2\text{PO}_4^-$  in aqueous solution. According to the research,  $\text{H}_2\text{PO}_4^-$  is a scavenger of  $\text{h}^+$  and  $\cdot\text{OH}$ , and the mechanism is similar to  $\text{HCO}_3^-$ . Therefore, the addition of  $\text{Na}_3\text{PO}_4$  to the reaction solution will significantly inhibit the photocatalytic degradation rate and degradation efficiency of SMX.

#### **Text S11 Mineralization Rate, Stability and Cyclic Experiment.**

When the degradation time of SMX reached 6.5 h, 41.49% SMX molecules were completely converted into  $\text{CO}_2$  and  $\text{H}_2\text{O}$ . Qiu et al. prepared  $\text{Fe}_3\text{O}_4/\text{Co}_3\text{O}_4$  nanosheet arrays on foamed nickel for the photocatalytic degradation of SMX, and the removal rate of TOC was 31.5%. It was shown that the mineralization rates of SMX by ozone and ozone/ $\text{H}_2\text{O}_2$  systems were 36.7% and 44.4%, respectively. Through comparison, it can be inferred that ZnO/ZIS has a higher mineralization degree of SMX under 500-W visible light irradiation for 6.5 h.

Through analyzing the data, it was clear that the leaching rates of  $\text{Zn}^{2+}$  and  $\text{In}^{3+}$  were 3.42% and 1.08%, respectively, after the photocatalytic degradation of SMX by ZnO/ZIS for 6.5 h, which may be caused by the partial acidity of the reaction system. The leaching rate of  $\text{Zn}^{2+}$  is slightly higher than that of  $\text{In}^{3+}$ , because of Zn being more active than In. It can be seen from the above results that ZnO/ZIS has good stability during the photocatalytic degradation of SMX.

Due to the cyclic experiment being carried out at 30 °C, the degradation effect of SMX was slightly different from that under the optimal experimental conditions. For each cycle, the degradation efficiency of SMX decreased by about 4%. After the four-time cycle experiments, the degradation efficiency of SMX could still reach 71.5%. This result verified that the ZnO/ZIS composite photocatalyst has good stability and could be reused in practical application.

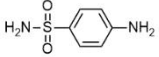
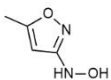
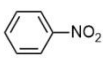
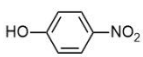
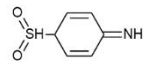
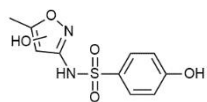
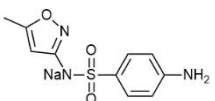
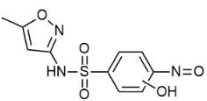
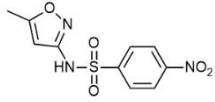
**Table S1** Gradient elution conditions

Time (min)	Current Speed (mL/min)	A(%)	B(%)
00.00	0.20	80	20
03.00	0.20	80	20
06.00	0.20	10	90
09.00	0.20	10	90
12.00	0.20	80	20
15.00	0.20	80	20

**Table S2** BET data for ZnO, ZIS, ZnO/ZIS

Material	BET (m <sup>2</sup> /g)	Pore Volume (cm <sup>3</sup> /g)	Average Aperture (nm)
ZnO/ZIS	118.30	0.20	4.88
ZIS	138.52	0.28	5.16
ZnO	42.09	0.15	23.42

**Table S3** Structure of degradation products of SMX by ZnO/ZIS

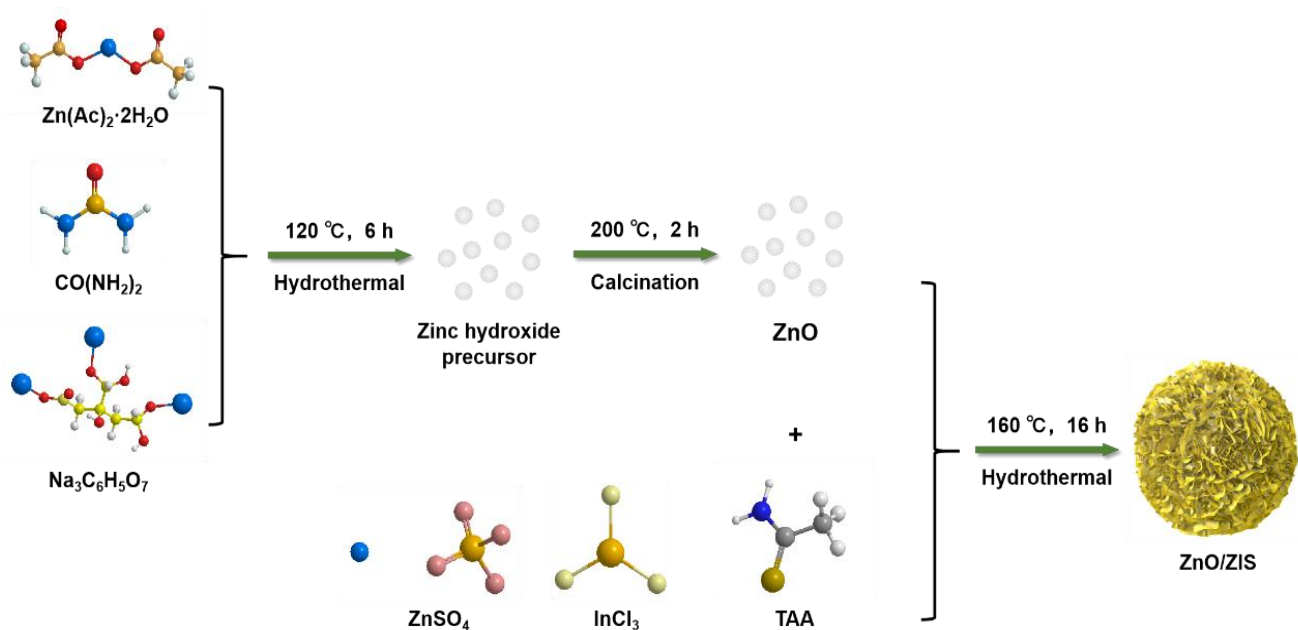
Product	Chemical Formula	Measured Value (m/z)	Literature Value (m/z)	Possible Structural Formula
P1	C <sub>6</sub> H <sub>6</sub> N <sub>2</sub> O <sub>2</sub> S	96.08	97	
P2	C <sub>4</sub> H <sub>6</sub> N <sub>2</sub> O	98.98	98.9	
P3	C <sub>3</sub> H <sub>3</sub> N <sub>2</sub> O <sub>2</sub>	114.09	114	
P4	C <sub>6</sub> H <sub>5</sub> NO <sub>2</sub>	124.08	123	
P5	C <sub>6</sub> H <sub>5</sub> NO <sub>3</sub>	139.98	139	
P6	C <sub>6</sub> H <sub>5</sub> NO <sub>2</sub> S	155.04	155.9	
P7	C <sub>10</sub> H <sub>11</sub> N <sub>2</sub> O <sub>5</sub> S	270.10	271.03	
P8	C <sub>10</sub> H <sub>10</sub> N <sub>3</sub> O <sub>3</sub> S	275.03	275.9	
P9a	C <sub>10</sub> H <sub>9</sub> N <sub>3</sub> O <sub>5</sub> S			
P9	C <sub>10</sub> H <sub>9</sub> N <sub>3</sub> O <sub>5</sub> S	283.71	283	
P9b	C <sub>10</sub> H <sub>10</sub> N <sub>3</sub> O <sub>5</sub> S			

**Table S4** The absolute energy of P9a gas molecules, the absolute energy and adsorption energy of P9a on ZnO(001)/ZnIn<sub>2</sub>S<sub>4</sub>(102) heterojunction surface

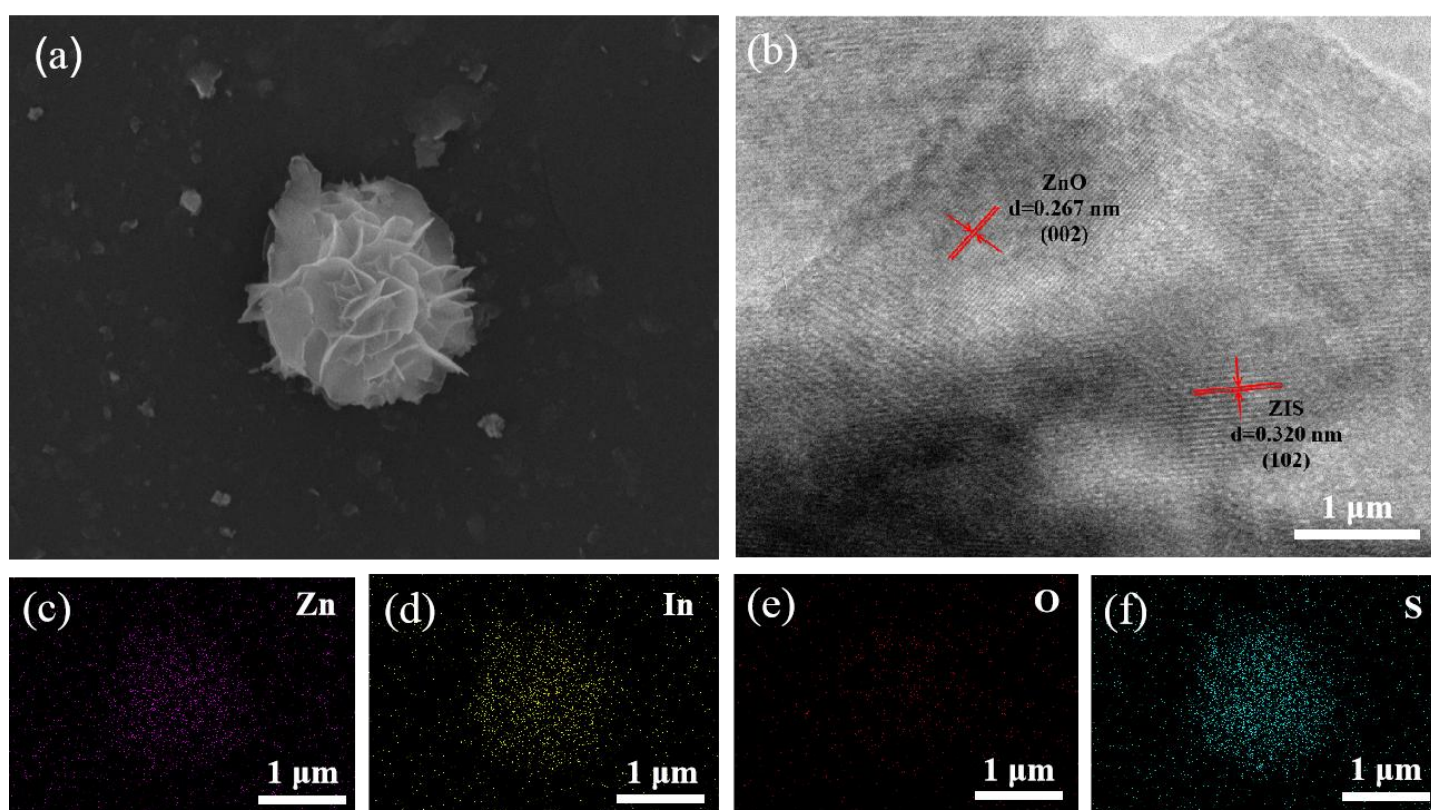
Gas molecules		ZnO(001)/ZnIn <sub>2</sub> S <sub>4</sub> (102) heterojunction		
molecule	E <sub>tot</sub> (eV)	adsorbate	E <sub>tot</sub> (eV)	E <sub>ads</sub> (eV)
P9a(g)	-185.684	*	-890.930	
		P9a on ZnO side	-1085.751	-2.03
		P9a on ZnIn <sub>2</sub> S <sub>4</sub> side	-1086.454	-1.65

**Table S5** Leaching rate of metal ions after degradation of SMX by ZnO/ZIS

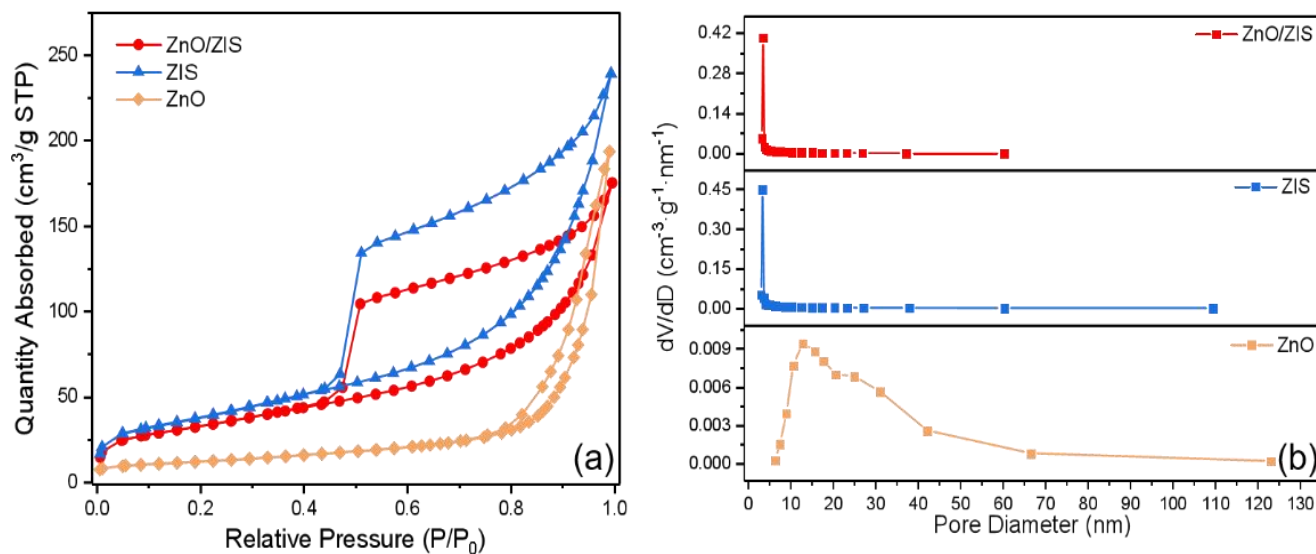
Ion species	Zn <sup>2+</sup>	In <sup>3+</sup>
SMX	3.42%	1.08%



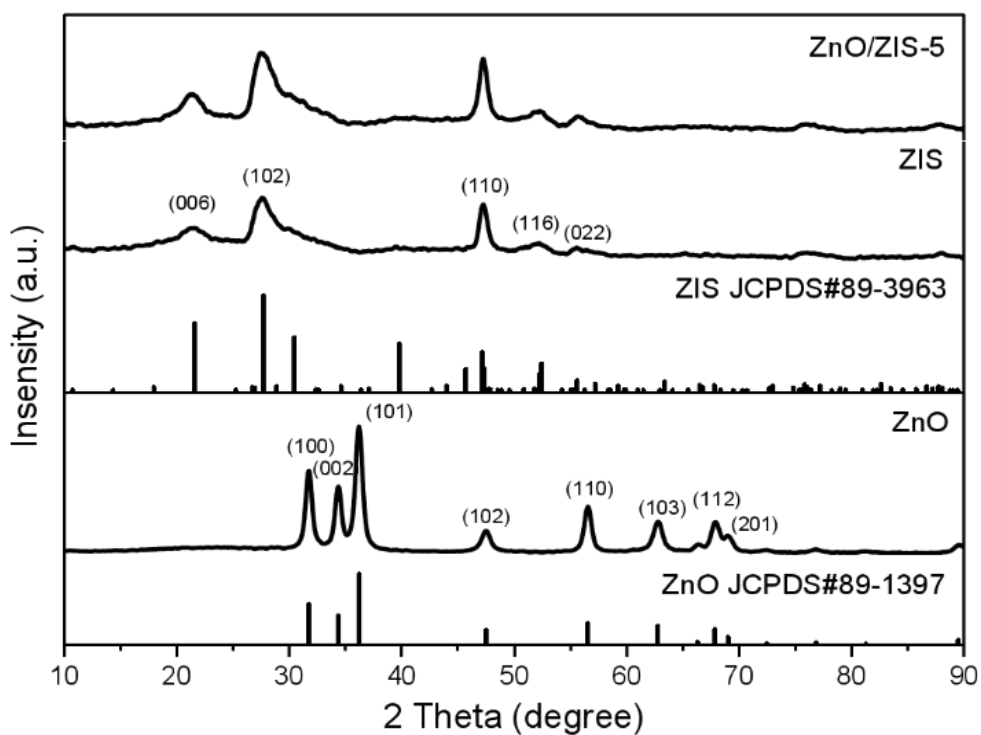
**Figure S1** Schematic diagram of preparation process of ZnO/ZIS.



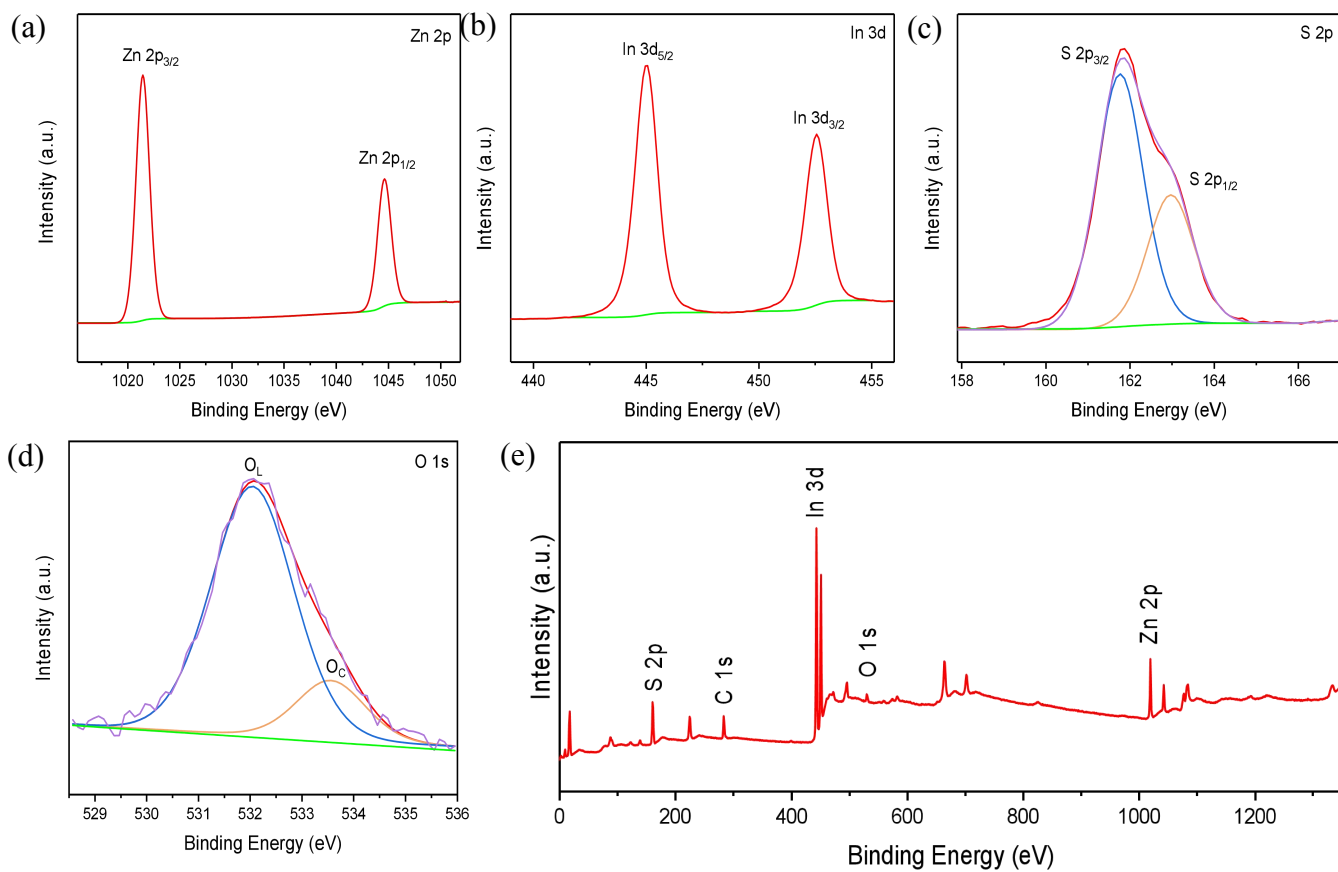
**Figure S2** SEM image (a); TEM image (b); EDS layered image (c)(d)(e)(f) of ZnO/ZIS.



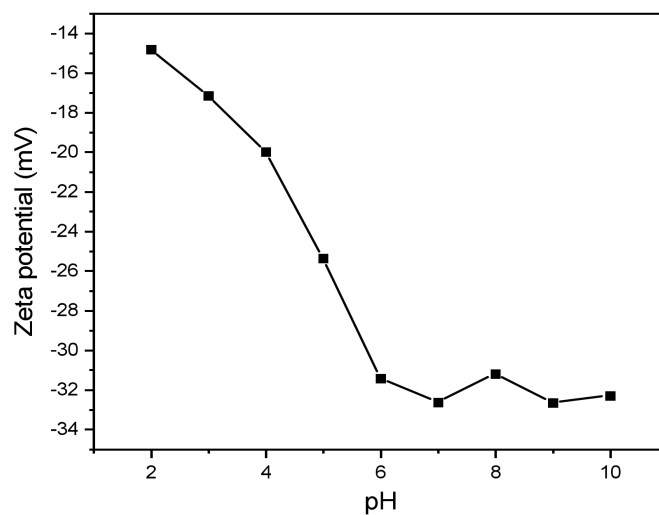
**Figure S3.** Nitrogen adsorption-desorption isotherms (a) and pore size distribution map (b) of ZnO, ZIS, ZnO/ZIS.



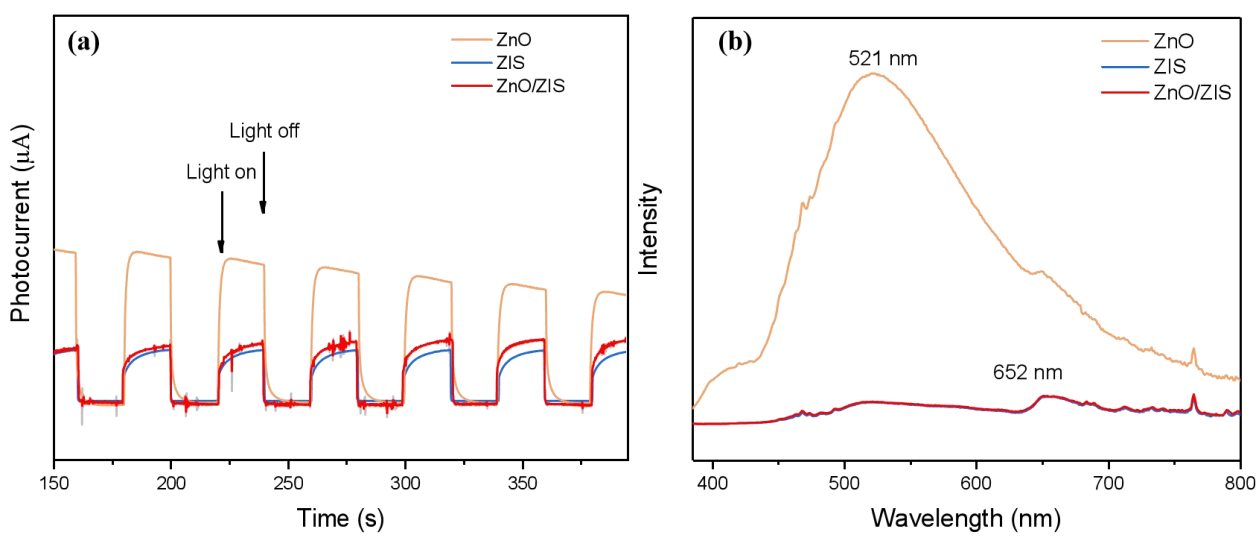
**Figure S4** XRD patterns of ZnO, ZIS, ZnO/ZIS.



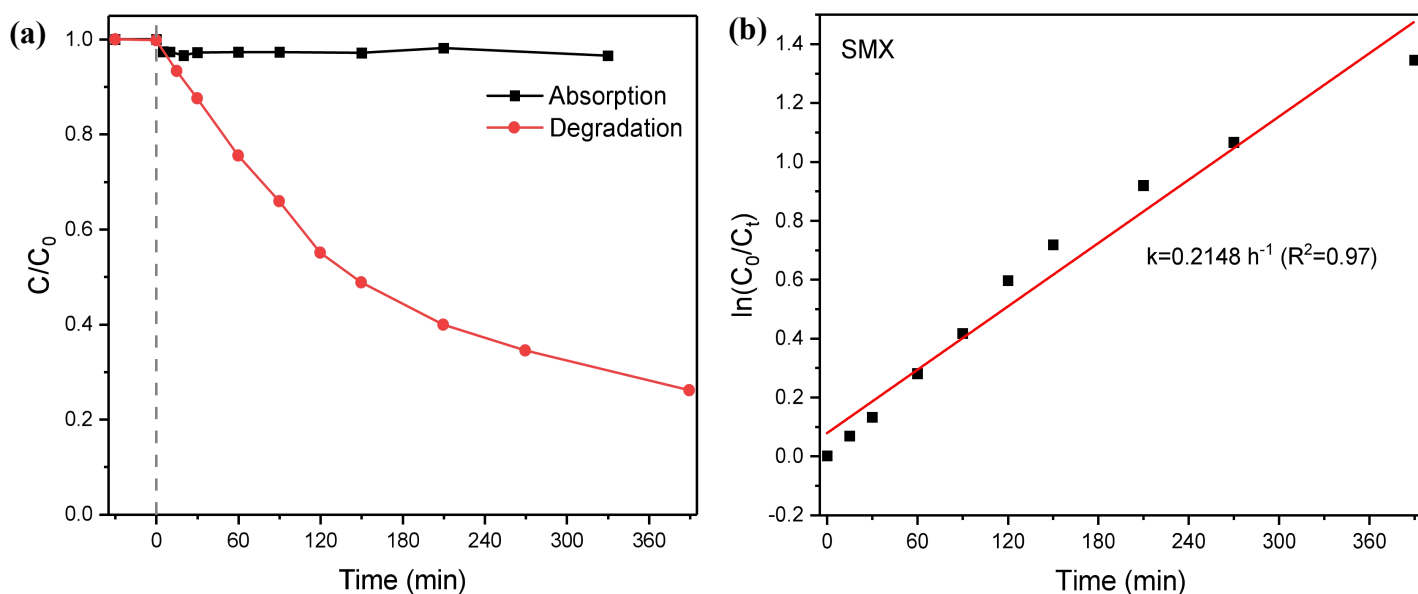
**Figure S5** XPS spectra of ZnO/ZIS heterostructure, (a) survey of the sample, (b) Zn  $2p$ , (c) In  $3d$ , (d) S  $2p$  and (e) O  $1s$ .



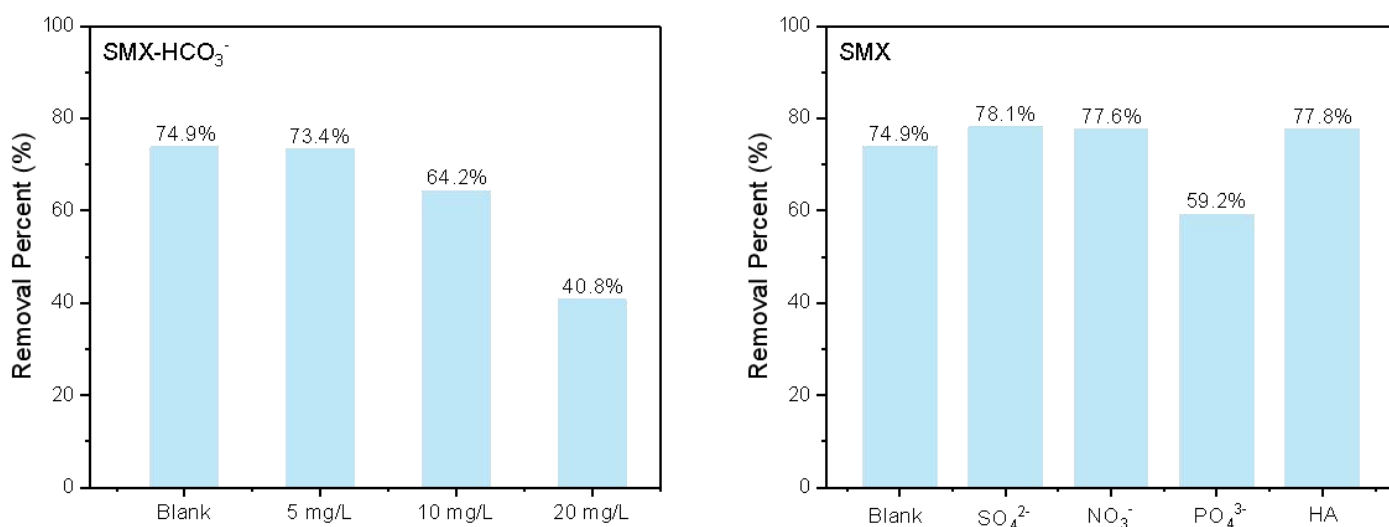
**Figure S6** Zeta potentials of ZnO/ZIS.



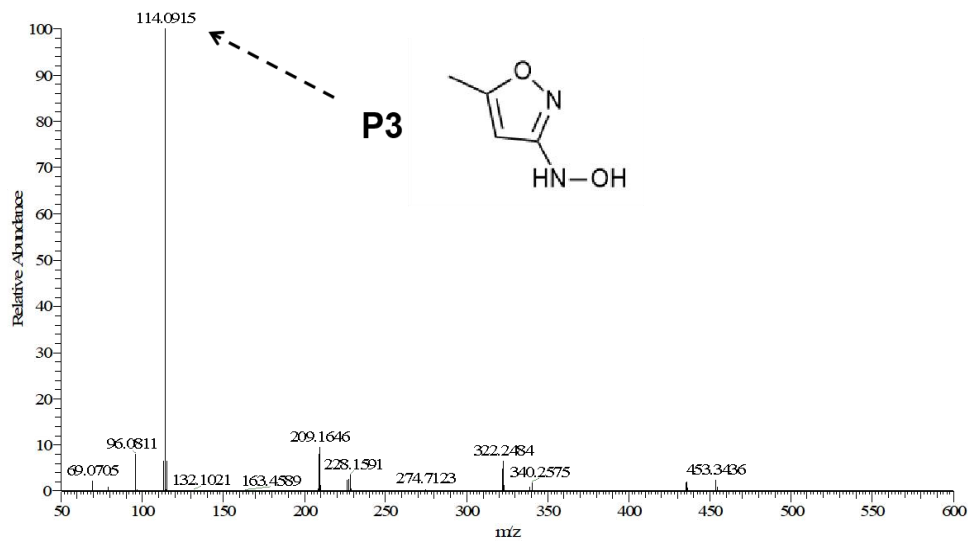
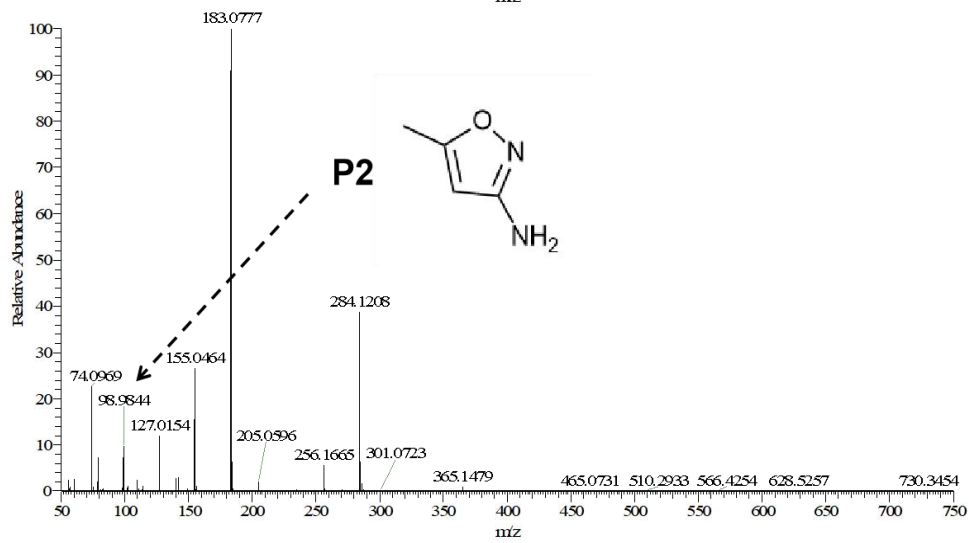
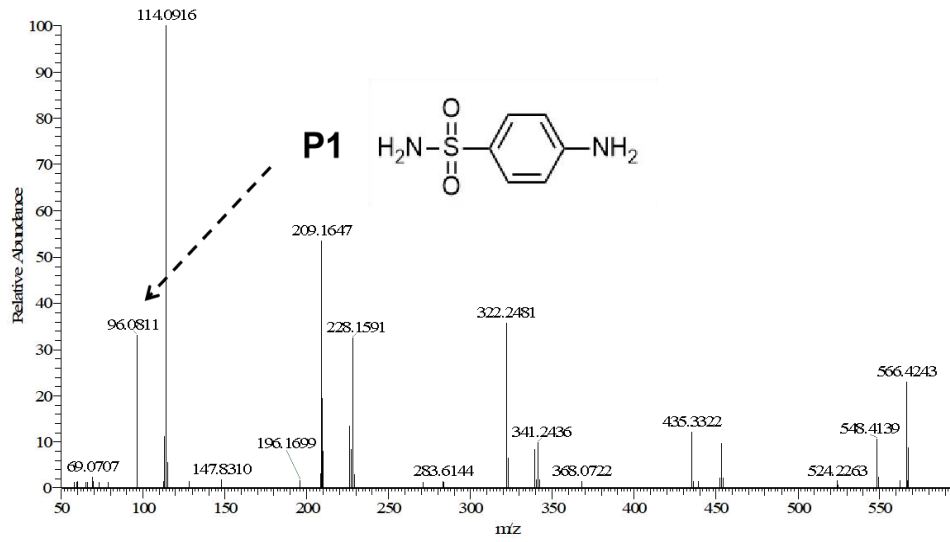
**Figure S7** (a) The i-t diagrams of ZnO, ZIS and ZnO/ZIS and (b) the photoluminescence spectra of ZnO, ZIS and ZnO/ZIS at an excitation wavelength of 376 nm.

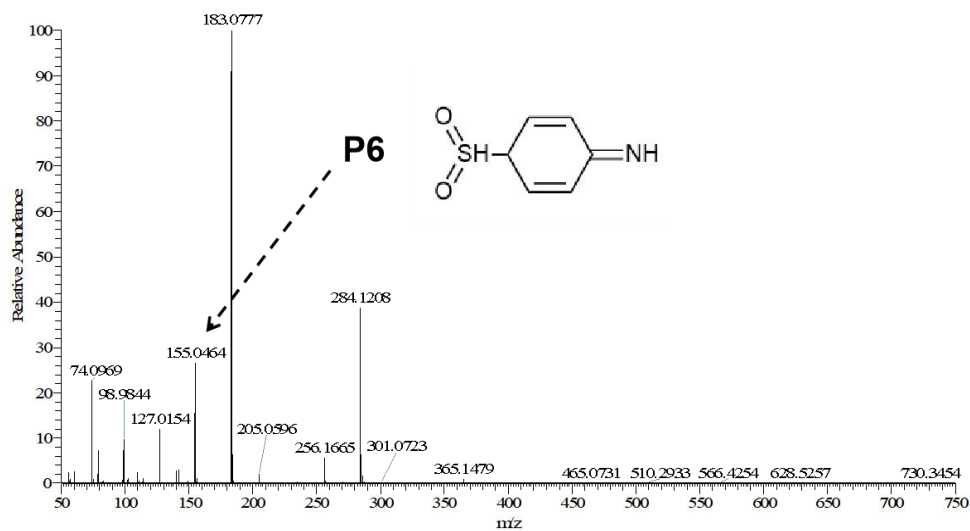
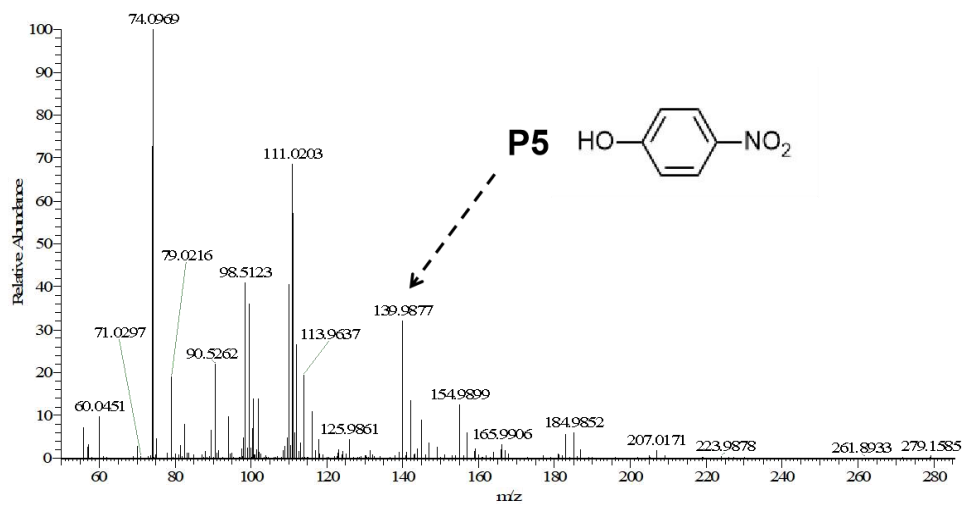
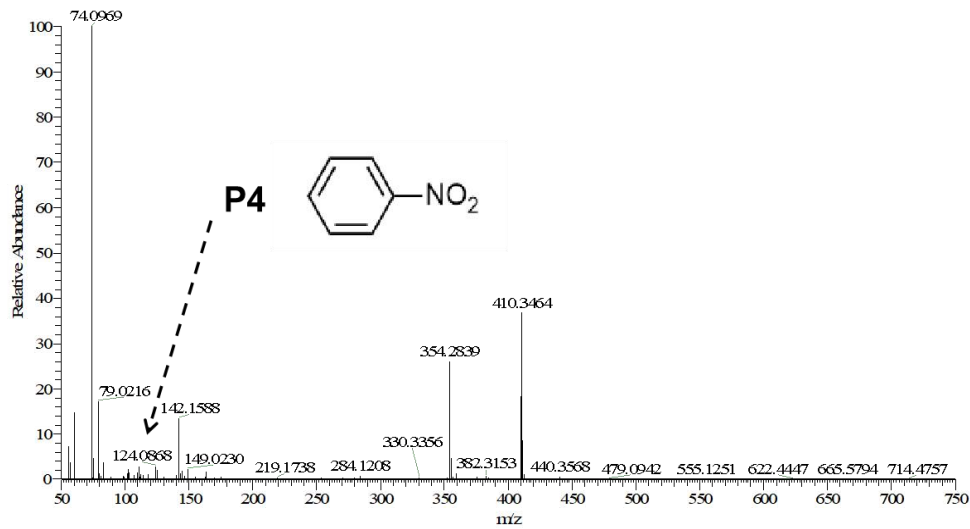


**Figure S8** (a) Photodegradation kinetics and dark adsorption process of SMX under 500 w visible light, (b) The  $K_{obs}$  of SMX degradation by ZnO/ZIS. Conditions:  $[SMX]_0=2.5 \text{ mg/L}$ ,  $0.20 \text{ g/L}$  dosage,  $\text{pH}=5.0$ ,  $500 \text{ w}$ ,  $15\text{-}20^\circ\text{C}$ .



**Figure S9** Effect of common anions and humic acids in water on the degradation of SMX(a)(b) by ZnO/ZIS. Conditions: (a)(b)  $[SMX]_0=2.5 \text{ mg/L}$ ,  $0.20 \text{ g/L}$  dosage,  $\text{pH}=5.0$ ,  $500 \text{ w}$ , room temperature.





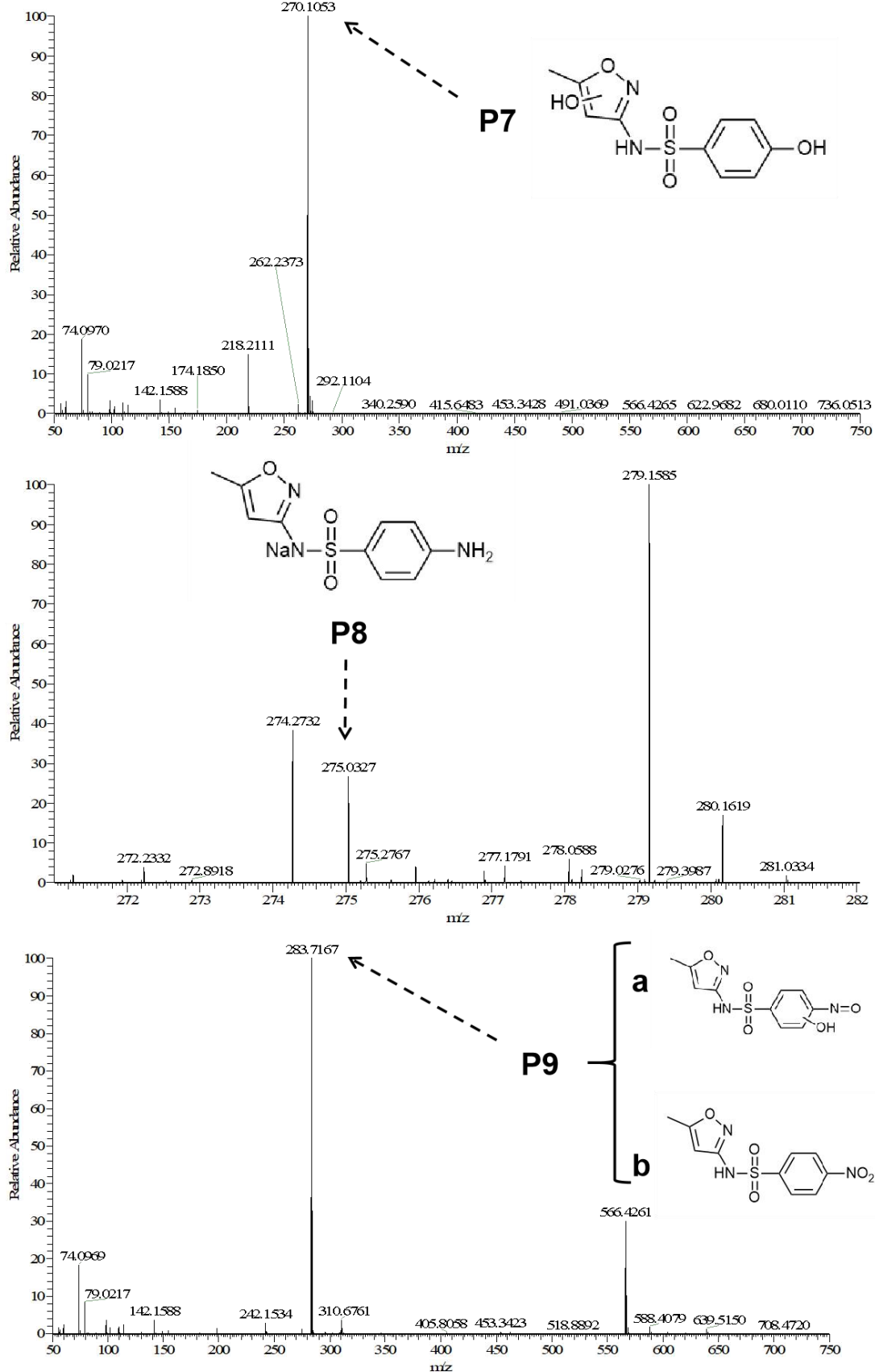


**Figure S10** The mass spectrum data and possible structures of 9 main products after ZnO/ZIS-5 degradation of SMX

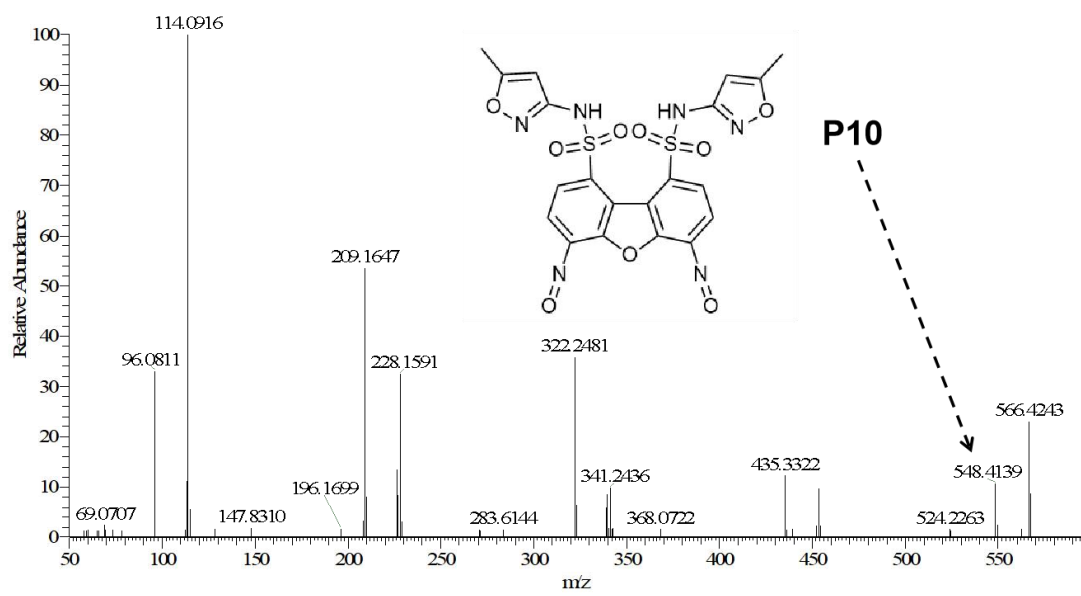


**Figure S11** Mass spectrum of degradation product P10 of SMX

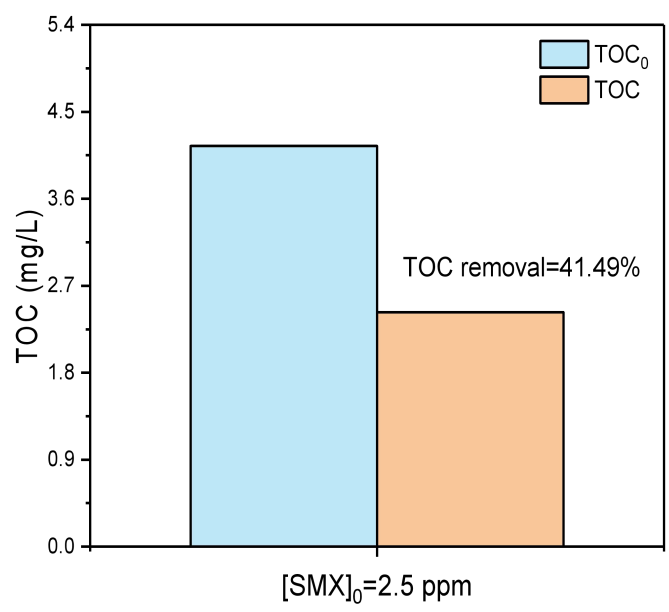


**Figure S12** The mineralization rate of ZnO/ZIS photocatalytic degradation of SMX

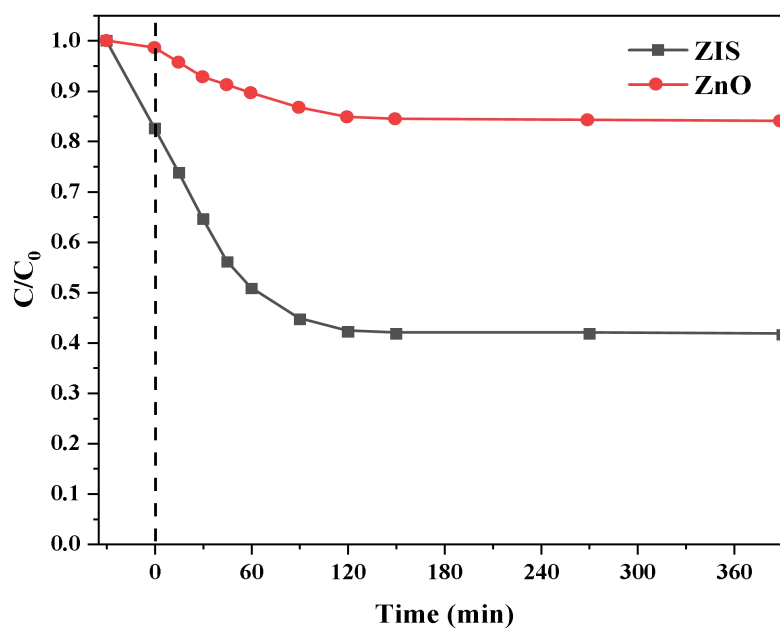


**Figure S13** The degradation efficiency of SMX using only ZnO and only ZnIn<sub>2</sub>S<sub>4</sub>.

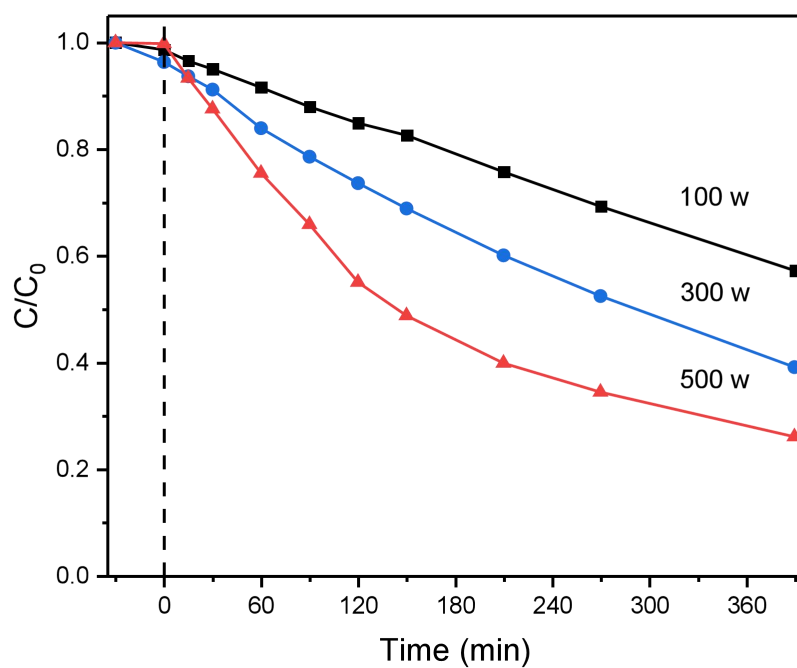


**Figure S14** The influence of light source intensity on the degradation of SMX by ZnO/ZnIn<sub>2</sub>S<sub>4</sub>.